Journal Name

ARTICLE

ABO_3 and $A_{1-x}C_xB_{1-y}D_y(O_{1-z}E_z)_3$: Review of Experimental Optimisation of Thin Film Perovskites by High-Throughput Evaporative Physical Vapour Deposition.

8Received 00th January 20xx,
Accepted 00th January 20xx

DOI: 10.1039/x0xx00000x

www.rsc.org/

Samuel Guerin*[a] and Brian E. Hayden[a,b]

The development of functional perovskites for future technologies can be achieved though the combinatorial synthetic method of evaporative Physical Vapour Deposition (HT-ePVD) which provides a direct low temperature route to anion stoichiometric materials. When combined with the ability to control and vary precisely the composition of thin film libraries of materials, high-troughput methods of screening and characterisation provides a rapid experimental determination of the structure / function relationship. This review of the use of HT-ePVD shows that controlled cationic substitutions in A and/or B sites can easily be explored, as can the effect of anionic substitution. This is exemplified in using this approach for a wide range of perovskite systems, where the tuning of the functional properties through cation substitution has application in a broad range of technologies.

Introduction

Naturally occurring perovskites are formed in abundance within the earth lower mantle, at depths between 660 and 2891 km with temperatures and pressures of up to 4000 °C and 139 GPa at the mantle – core boundary.[1] Perovskites are an abundant natural mineral, with 93 % of the earth's lower mantle and 38 % of the earth, by mass, being made up perovskites, $MgSiO_3$ the commonest.[2] However, these are limited to the high pressure of the earth's lower mantle and are not stable at ambient conditions. On the surface the mineral $CaTiO_3$ was the first perovskite discovered in 1839. However, its interest and usage as a natural mineral has been limited. Following characterisation, in 1926, of the crystal structure of calcium titanate[3] and realisation of the ability to substitute, within the crystal structure, a large range of cations and anions, perovskites have received a large amount of attention due to their broad range of applications. From dielectrics to electrical conductors, their properties and usefulness become evident as their composition and crystal symmetry changes. Non-linear dielectrics become tunable enabling their use in microwave applications. The creation of localised electrical dipoles leads to polarizability, ferroelectricity and piezoelectricity. Disorder and the creation of vacancies allow for ionic transport. Perovskites can also be used as catalysts in fuel cells for oxygen reduction and oxygen evolution reactions.[4-8] Indeed, perovskites materials find applications in photovoltaics[9-13], superconductors[14-17], giant magneto-resistors[18-20], LEDs[21-25] and lasers.[26, 27] We describe here how combinatorial synthesis by ePVD provides the first step in a flexible and powerful high throughput methodology in optimising the function of perovskites.

Usually perovskites are made of alkaline earth or rare earth metals in A sites and transition metals in B sites and the anions are mostly oxygen, although many perovskites can also be formed using other anions from the halogen group. The A sites occupy the corners of the unit cell with a coordination number of 12 to the anions, whilst the B sites occupy the centre of the unit cell with a coordination number of 6. The anions form a network of octahedra and their ability to be tilted is linked to many of the properties observed in dielectric behaviours. The Goldschmidt tolerance factor using the relative size of the ionic radii of atoms allow to predict the existence of perovskite structures. Some articles[28, 29] summarise the possible use of the elements in the three different sites of the perovskite structure in the form of a periodic table. These are useful starting points when embarking on high-throughput discovery of perovskite materials with multiple elements.

Under ideal circumstances perovskites exhibit a pseudo-cubic structure and distortions and variations in composition reduce the crystal symmetry to form tetragonal, rhombohedral and monoclinic crystal structures. Most studies focus on the study of balanced perovskite where the A/B sites ratio equals one, however our compositional spread approach allows to probe the compositional spread further by easily achieving $A_xB_yO_{3-\delta}$ stoichiometries.

Being the subject of so many studies and such a large number of applications, many routes are used for the synthesis of perovskites. Bulk perovskite can be synthesised by classical approaches such as solid phase reactions of common reagents, solution synthesis using organometallic precursors[30]. Other techniques such as hydrothermal

[a] *Ilika Technologies Ltd. Kenneth Dibben House, Enterprise Road, University of Southampton Science Park, Chilworth, SO16 7NS.*
[b] *Chemistry, The University of Southampton, Highfield, SO17 1BJ*

† Footnotes relating to the title and/or authors should appear here.
Electronic Supplementary Information (ESI) available: [details of any supplementary information available should be included here]. See DOI: 10.1039/x0xx00000x

processing[31-33], sol-gels[34-37] or mechanochemical[38-41] processes are also used to produce high quality perovskites. Similarly to how perovskites are made in the natural world, high pressures are also used for their synthesis.[42] If not already necessary during the synthesis steps, most of these methods (apart from hydrothermal processing) will require elevated sintering conditions to finalise the synthesis step and produce high density materials. Thin film perovskites have been synthesised using CVD[11, 13, 43, 44], ALD[12, 45-48], PLD[49-57], CSD[58, 59]sputtering[60, 61] and evaporative PVD[10]. However, most of these studies focus on single compositions perovskites or a few discreet compositions. In terms of using a high throughput approach, a number of studies refer to computational methods making use of a limited number of experimental points for comparison[62-70]. Approaches allowing the rapid synthesis and screening of perovskite materials with extended variation in the compositional space are limited by the synthesis method used [54, 56, 57, 59-61, 71-76]. Where some control of the cationic concentrations can be achieved by combinatorial methods, the necessity to employ high temperatures to ensure crystallisation can lead to a difficulty in achieving stoichiometric anionic concentrations.

Perovskites systems studied by HT-ePVD

In our approach, we are able to fully control the compositional spread of the cations enabling multiple substitutions in either cationic sites, have some control of the anion site by being able to offer a mixture of elements and have control of the temperature at which synthesis takes place allowing control of the crystallinity of the thin films. This is due to the co-evaporation of the constituent elements in atomic form from the gas phases onto a moderately heated substrate. As the atomic vapours for each cation form a gradient of abundance across the substrate, each element is condensing on the substrate in the desired quantity to generate the target material. The relatively small distances atoms have to travel to achieve equilibrium ensure that minimal energy is required to form the target material, hence lower than typically used temperatures have been necessary using this technique. The anions are provided via an atom source which enables the dissociation of the diatomic molecules into more reactive atomic species, these have a high chemical potential allowing for the relatively easy formation of stoichiometric perovskites. Furthermore, the synthesis method will ensure that the anion concentration is balanced with the cation concentration as the system minimised its energy during synthesis. All these allow an unprecedented access to the relationship existing between the properties under investigation and their compositional dependence. High-throughput evaporative Physical Vapour Deposition (HT-ePVD) offers the unique advantage of allowing to control most aspect of perovskites synthesis. Although ABO_3 is the stoichiometric target composition, careful preparation of the growth chambers allows to study the effect of elemental substitutions on each of the cationic sites independently or simultaneously. Furthermore, the use of an RF atom source to provide the anionic element can be used as a source of mixed anions thus enabling doping level investigations of the effect of mixed anions on the properties of the perovskites. It also allows to ensure stoichiometric concentrations of anions are provided during the synthesis for all compositions investigated.

This approach has been used for the last ten years to probe the relationship between composition, structure and key figures of merit of selected perovskites. As exemplified in this paper, perovskites used for piezoelectricity, such as $Pb_xZr_yTi_{1-y}O_{3-\delta}$[77, 78] and $Bi_xNd_{1-x}Fe_yO_{3-\delta}$[79], ferroelectricity in $Bi_xNa_{1-x}Ti_yO_{3-\delta}$[80, 81], tunable capacitors $Ba_xSr_{1-x}Ti_y0_{3-\delta}$[82], $Ba_xSr_{1-x}Ti_yO_{3-z}N_z$[82], $(Ba_{0.8-x}Gd_xSr_{0.2})_{1+x}(Ti_{1-p}Zr_p)_{1-x}O_{3-z}N_z$.[82] and $Ba_xSr_{1-x}Ti_yMn_{1-y}O_{3-\delta}$[83], lithium electrolytes as $La_xLi_{1-x}Ti_yO_{3-\delta}$[84] and electrocatalysis with $Sr_xTi_{1-y}Fe_yO_{3-\delta}$[4], $La_xCa_{1-x}Mn_yO_{3-\delta}$[5] and $La_xMn_yNi_{1-y}O_{3-\delta}$[5] have all been studied using this approach. This broad range of applications have all required different type of substitution on either A-sites, B-sites, anionic sites or a combination of all the above.

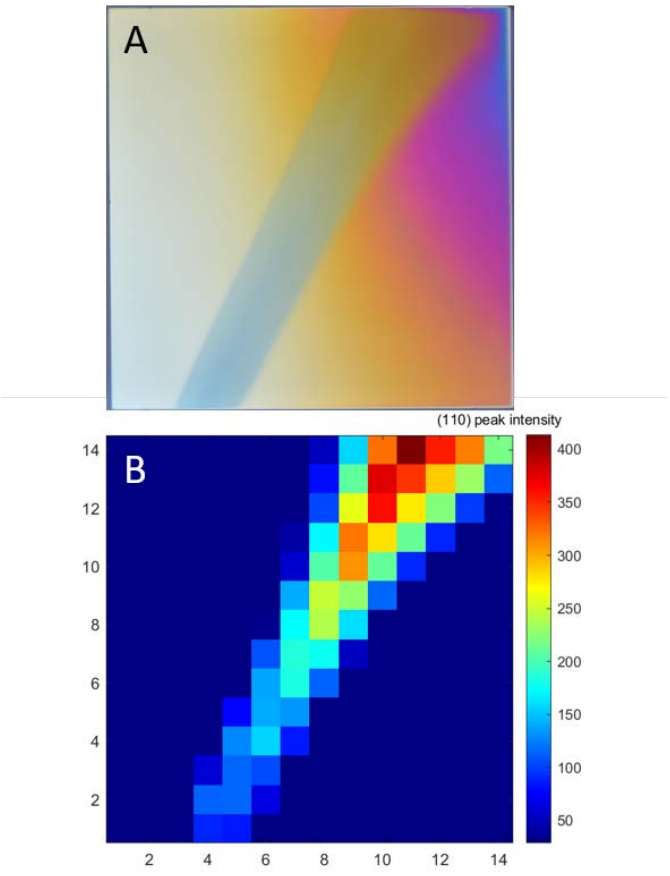

Figure 1: sample photograph (A) and array map of the intensity of the (110) XRD reflection (B) of a $La_xCa_{1-x}Mn_yO_{3-\delta}$ library showing the link between the optical observation of the perovskite and its existence as shown by XRD (system studied as part of the work published in Bradley *et al.*[5]).

Equation 1 describes the adaptation of the tolerance factor calculation used for the systems presented. It is based on the assumption of an $A_xB_{1-x}O_3$ overall stoichiometry with r_A, r_B and r_O the ionic radii of the A-site, B-site and anionic sites, respectively, in their

expected coordination, [A_i] and [B_i] are, respectively, the concentration, in at%, of the A-site and B-site constituents.

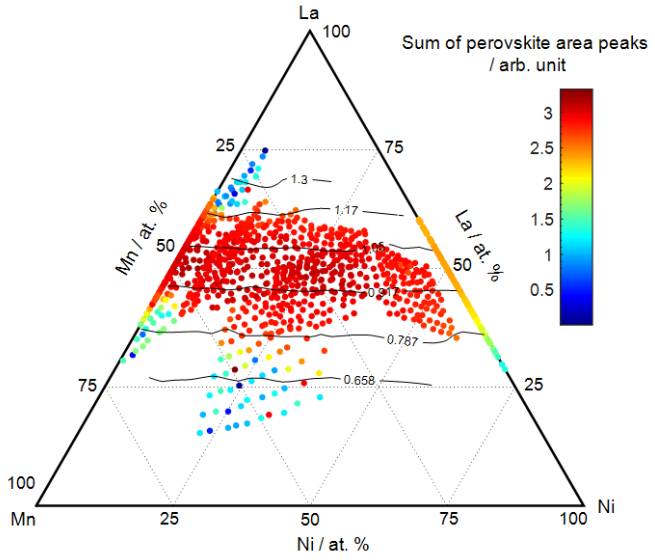

Figure 2: Domain of existence of the $La_xMn_yNi_{1-y}O_{3-\delta}$ perovskite structure as function of composition. Existence expressed as the log of the sum of the area of the XRD peaks. Calculated values of the Goldsmith tolerance factor overlay on the ternary showing existence of the perovskite for 0.8 < t < 1.2 (system studied as part of the work published in Bradley *et al.*[5]).

Synthesis

All systems presented have been synthesised using a high-throughput evaporative physical vapour deposition system using a system of independent wedge shutters and sources allowing the co-deposition of the constituent elements.[85] All elements were evaporated from their pure solid forms by generating a vapour allowing the control of their relative deposition rates. The cations were usually contained in crucibles and loaded using either Knudsen cells or electron gun sources depending on the temperature required to achieve a sufficient deposition rate. Anions were provided by feeding a flux of pure (or mixed) molecular atoms to an RF atom source where a plasma contained within a discharge tube allow for the splitting of the di-atomic molecules into a mixture of molecules, ions, charged radicals and neutral atoms. This mixture being much more reactive than the molecular gas allow for the synthesis of anion stoichiometric compounds: The anions were provided in excess of the cations, at all positions of the substrate, in order to favour the stoichiometric compounds to be formed for a given cationic concentration. The syntheses presented here were carried out mainly on platinised substrates at a moderate temperature, (followed by an annealing step to ensure formation of the perovskite structure) or by direct synthesis at an elevated substrate temperature to favour the in-situ growth of the crystalline phase as the elements are being deposited. In brief, the relative rates of the constituent elements along with their gradients, achieved by the wedge shutters, govern the compositional spread achieved in the resulting thin films, whilst the substrate temperature allows to access in situ, or facile, formation of the crystal structure.

(eq. 1)
$$t = \frac{\left(2\sum_i [A_i] \times r_{A_i} + r_O\right)}{\sqrt{2}\left(2\sum_i [B_i] \times r_{B_i} + r_O\right)}$$

Figure 1 shows the link between an actual photograph (A) of a $La_xCa_{1-x}Mn_yO_{3-\delta}$ perovskite thin film sample and the map of intensity of the (110) reflection obtained by XRD (B). In this particular sample the domain of existence of the perovskite extends from 40 at% up to 56.6 at% of B-site atoms (Mn in this instance). This corresponds to a Goldschmidt tolerance factor between 0.81 and 0.96 using standard ionic radii, coordination numbers and averaged oxidation state of Mn. This variation in the tolerance factor agrees with the reported observation of both rhombohedral and cubic crystal structures. A region with a particular optical reflectivity is observed corresponding to the region of the perovskite phase. Outside of this region, the sample remained amorphous and no inhomogeneity is observed, the colour variation between the two regions appears as a shift / discontinuity and, since the sample thickness is only of the order of 100 nm, the changes could be attributed to changes in the absorption and refractive indexes of the material between the amorphous and the crystalline states or to sudden variation in thickness if the material's density is affected by the change of crystal state. The domain of existence of the perovskite is restricted to a tolerance factor between 0.81 and 0.96 for this particular system and for the synthetic method used (the samples were deposited by in-situ crystallisation through co-deposition of constituent elements on a substrate at 550 °C) which is relatively limited for our synthetic approach. Perovskite usually exist with Goldschmidt tolerance factors (t) between 0.7 and 1.0 and their crystal structure can be linked with its value.[9] The ideal cubic structure is reported to correspond to t between 0.9 and 1.0 whereas distorted perovskites exits for t between 0.7 and 0.9. For other systems synthesised and studied using our approach[5, 82] we have observed perovskites for the whole range of composition synthesised with a corresponding Goldsmith tolerance factor between 0.82 and 0.98. More remarkable is the fact that using our synthesis method we are able to obtain perovskite structures for t>1, when at these values non-perovskites structures are normally reported[9]. For the $Ba_xSr_{1-x}Ti_yO_{3-z}N_z$ pure perovskite was reported for t up to 1.05 and mixed phase above that. A more remarkable domain of existence is highlighted in the ternary plot of Figure 2 where the log of sum of the area of the diffraction peaks of the perovskite is plotted against composition and overlaid with the calculated tolerance factor. From this figure we can infer that, for the $La_xMn_yNi_{1-y}O_{3-\delta}$ system, a perovskite can be formed for tolerance factor between 0.8 and 1.2.

As mentioned before, the formation of the perovskites was usually done by either, deposition at moderate temperature followed by annealing to ensure crystallisation or by in-situ deposition to allow direct formation of the perovskite structure as the elements are evaporated and the film grown. Generally, the range of compositions for which the perovskites is observed is greater for the direct in-situ crystal growth method than in the case of the post deposition annealing approach. Furthermore, trends attributable to the variations in the relative ratios of A-sites and B-sites cations become more apparent and extend more easily to super and sub stoichiometry of the anions in the case of in-situ crystal growth compared to post deposition annealing. Therefore, when experimentally possible, it is preferred to synthesise the perovskites by in-situ direct crystallisation.

A-site substitutions

A-site substitution has been the commonest approach with the studies of $Bi_xNa_{1-x}Ti_yO_{3-\delta}$ as ferroelectrics[80, 81], $Bi_xNd_{1-x}Fe_yO_{3-\delta}$ as piezoelectric[79], $Ba_xSr_{1-x}Ti_yO_{3-\delta}$ as tunable dielectrics[82], $La_xLi_{1-x}Ti_yO_{3-\delta}$ as lithium ion conductor[84] and $La_xCa_{1-x}Mn_yO_{3-\delta}$ as electrocatalysts.[5]

Synthesis of the $Bi_xNa_{1-x}Ti_yO_{3-\delta}$, $Bi_xNd_{1-x}Fe_yO_{3-\delta}$ and $La_xLi_{1-x}Ti_yO_{3-\delta}$ systems was done by depositing the constituent elements at moderate substrate temperature resulting in amorphous thin films which required a post deposition annealing step to form the perovskite structure. For the $Ba_xSr_{1-x}Ti_yO_{3-\delta}$ and $La_xCa_{1-x}Mn_yO_{3-\delta}$ the perovskite was formed by direct in-situ crystal growth achieved by deposition of the elements at elevated substrate temperatures (650 °C for $Ba_xSr_{1-x}Ti_yO_{3-\delta}$ and 550 °C for $La_xCa_{1-x}Mn_yO_{3-\delta}$).

In the case of the $Bi_xNa_{1-x}Ti_yO_{3-\delta}$ system[80] a map of the dielectric constant variation (see Figure 3) shows a gradual increase from Ti rich compositions toward a maximum for the ideal cation ratio at 50 at% Ti, past this line there is a sudden decrease in the measured dielectric constant. A region of relatively high dielectric constant is observed for around 30 at % Bi, 20 at% Na and 50 at% Ti (excluding oxygen) and it is surrounded by regions where little to no polarisation is measured.

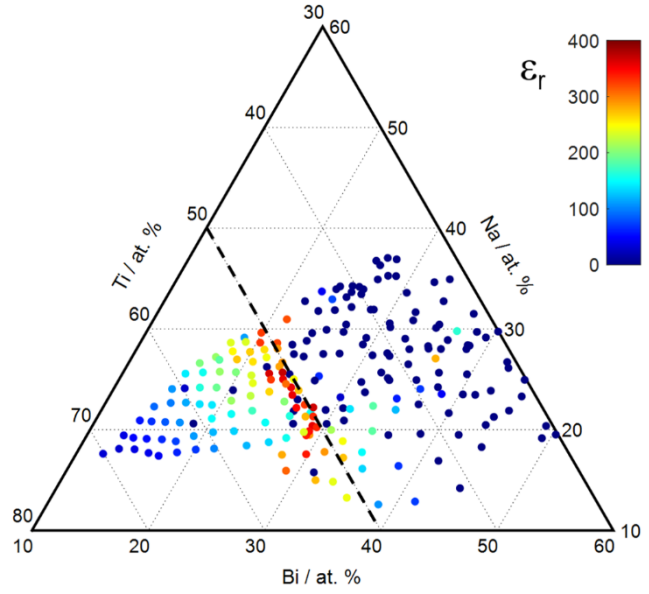

Figure 3: Dielectric constant for the $Bi_xNa_{1-x}Ti_yO_{3-\delta}$ system following anneal in air at 700 C.[80]

Piezoelectricity at room temperature was the focus of the study in the $Bi_xNd_{1-x}Fe_yO_{3-\delta}$ system[79] and its direct measurement by PFM was limited to the tie line of the ideal perovskite $Bi_xNd_{1-x}FeO_3$, a phase transition was identified between a R3c and Pnma crystal structure with a region of mixed phases for $0.12 < x < 0.2$, and an increase in piezoelectric response was observed with a maximum at around x = 0.11. It was concluded that the maximum was linked to the boundary between the single R3c phase and the mixed phase region caused by a softening of the lattice in the vicinity of the phase boundary.

The $La_xLi_{1-x}Ti_yO_{3-\delta}$ system was studied for its properties as Li ion conductor[84], its synthesis was achieved by post deposition annealing of the thin films and multiple samples were required to allow for a computational analysis of the experimental data obtained which yielded a hotspot for ionic conductivity (5.45×10^{-4} S cm^{-1} for $Li_{0.17}La_{0.29}Ti_{0.54}$ (excluding oxygen)). The mechanism for Li ion mobility within the structure is due to the large number of vacancies within the perovskite structure as this is reflected in its more common formula of $Li_{3x}La_{(2/3)-x}\square_{(1/3)-2x}TiO_3$ ($0 < x < 0.16$).[86]

The dielectric properties of $Ba_xSr_{1-x}Ti_yO_{3-\delta}$ were investigated for its application in antenna as tunable dielectric.[82] This application requiring thin film as final product ensure that the study's findings have direct bearing on product development. This system was synthesised by direct in-situ crystallisation, with a substrate temperature of 650 °C, leading to entire sample libraries with wide compositional spread exhibiting pure perovskite phases. The resulting dielectric map obtained is shown in Figure 4, it shows a region of higher dielectric constants for Ba rich compositions, compared to Sr, and these are found for slight excess Ti (with respect to the target 50 at% perovskite). For this system a tunability ratio of 4.9 was achieved between 0 and 36 kV mm^{-1}.

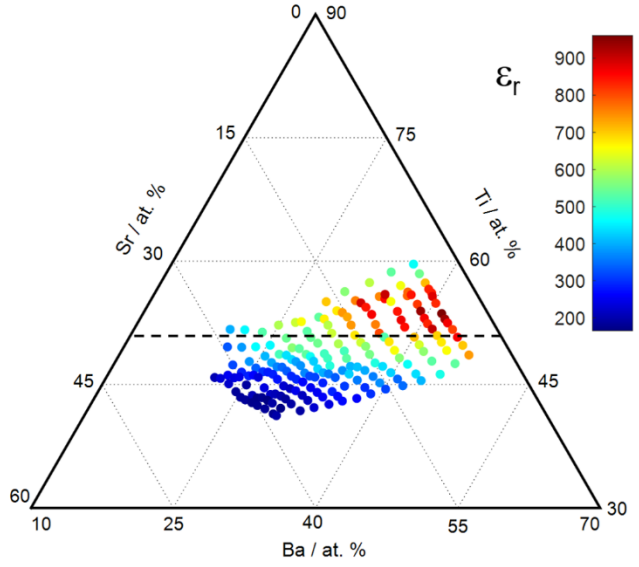

Figure 4: Dielectric constant for the $Ba_xSr_{1-x}Ti_yO_{3-\delta}$ system, the dashed line represents the 50 at% Ti (results obtained as part of the work published by David *et al*.[82]).

B-site substitution

B-site substitution studies have focussed on studying the $Pb_xZr_yTi_{1-y}O_{3-\delta}$ solid solution for piezoelectric materials[77, 78] and $La_xMn_yNi_{1-y}O_{3-\delta}$ and $Sr_xTi_{1-y}Fe_yO_{3-\delta}$ as electrocatalysts.[4, 5]

The application of high-throughput thin film methodologies for the synthesis and study of perovskite materials was first developed using our approach for the study of piezoelectric materials such as lead zirconate – lead titanate with the exploration of the $Pb_xZr_yTi_{1-y}O_{3-\delta}$ solid solution.[77, 78] These libraries were made by post deposition annealing to obtain the perovskite structure. Analysis of the crystal structure via deviation from Vegard's law (see Figure 5 top) combined with Raman spectroscopy revealed a transition at 36 at% Ti (with respect to Zr) between a tetragonal phase (Ti rich) to a rhombohedral one (Zr rich). Thin film XRD proved unable to resolve the difference between the two crystal structures, both appearing pseudo cubic. The presence of this morphological phase boundary is similar to what is observed in bulk PZT although it is reported for bulk to happen for a Zr:Ti ratio of 0.53:0.47. The difference has been attributed to residual stress and smaller grain sizes.[78] For selected compositions along the solid solution the ferroelectric response was obtained with a clear trend of large polarisation for Zr rich compositions as shown in Figure 5 (bottom).

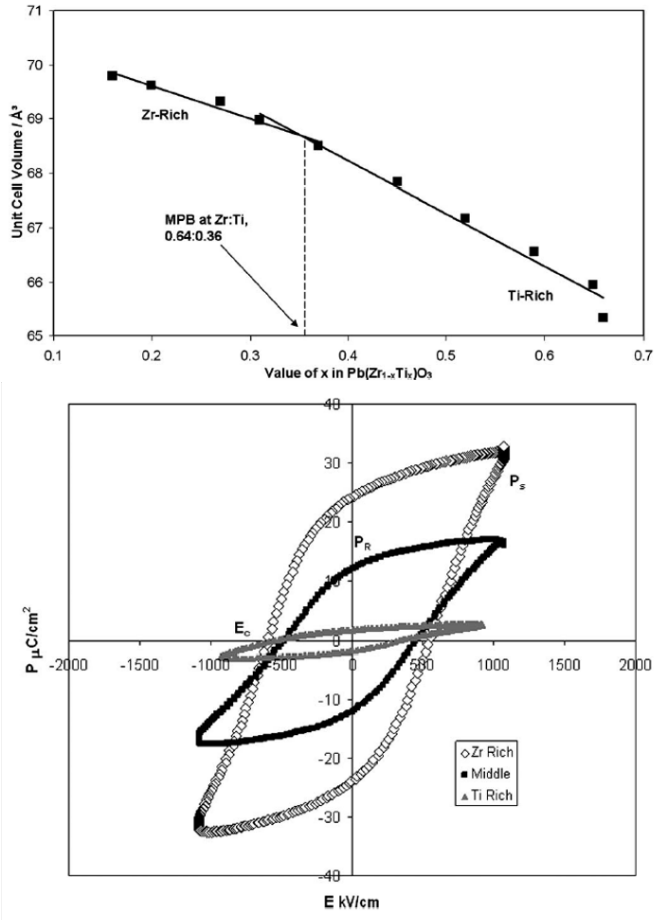

Figure 5: variation in unit cell volume (top) for the $PbZr_yTi_{1-y}O_3$ system. Ferroelectric loops for selected regions along the solid solution of $PbZr_yTi_{1-y}O_3$.[78]

Direct in-situ synthesis of B-site substitutions have been the focus of two studies with the purpose of optimising electrocatalysts used for Oxygen Evolution Reaction (OER) and Oxygen Reduction Reaction (ORR).[4, 5] In the case of the $Sr_xTi_{1-y}Fe_yO_{3-\delta}$[4], it was found that an extensive domain of existence of the perovskite was obtained by synthesis at 650 °C. Interestingly not only the range of compositions in the solid solution of $Sr_xTi_{1-y}Fe_yO_{3-\delta}$ achieved was larger using the ePVD method compared to traditional methods but also the temperature at which this was achieved is significantly lower. The extensive characterisation and testing undertaken in this system concluded that the OER was found to be optimal for the $SrTi_{0.5}Fe_{0.5}O_{3-\delta}$ composition as it offers the best compromise between catalytic activity and electrode stability. Furthermore, mechanisms involving oxygen vacancies are believed to be responsible for the relatively high activity of the materials. A similar synthetic approach was taken for the study of $La_xMn_yNi_{1-y}O_{3-\delta}$ system.[5] A relatively low substrate temperature of 550 °C was sufficient to ensure crystallisation of the perovskite structures along the lanthanum tie-line. The $La_xMn_yNi_{1-y}O_{3-\delta}$ system is found vary from cubic for $LaMnO_3$ to rhombohedral for $LaNiO_3$ with evidence of an unexpected A-site substitution of Mn^{2+} in $LaMnO_3$ and Ni^{2+} in $La_xMn_yNi_{1-y}O_{3-\delta}$. Electrochemical activity shows an expected anti-correlation between OER and ORR. However, in the case of the observed A-site substitution of Ni^{2+}, a correlation OER and ORR is observed, linked to the appearance of a Mn^{3+}/Mn^{4+} redox couple in the electrochemistry. The optimal reversible ORR/OER activity is observed for $La_{0.85}Mn_{0.7}Ni_{0.45}O_{3-\delta}$, a composition away from the tie line for a simple B-site substitution. This study was completed by the synthesis and study, in a similar manner, of the expected A-site substitution of $La_xCa_{1-x}Mn_yO_{3-\delta}$. This system was observed to vary from cubic to cubic for the end members via an orthorhombic crystal structure as La substitutes for Ca along the Mn tie-line. The results show that the substitution of La^{3+} for Ca^{2+} results in the appearance mixed valent perovskites with an optimum OER/ORR activity linked to the appearance of the Mn^{3+}/Mn^{4+} redox couple.

A and B site substitutions

The latest example shows the link between A and B site substitutions; the HT-ePVD synthetic approach allows also studies of both A and B sites substitutions simultaneously. This has been the focus of further optimisation of the BST tunable dielectric where the $Ba_xSr_{1-x}Ti_yMn_{1-y}O_{3-\delta}$ system was studied for its use in tunable co-planar waveguides for GHz applications.[83] Libraries of $Ba_xSr_{1-x}Ti_yMn_{1-y}O_{3-\delta}$ were synthesised by in-situ growth with a substrate temperature of 640 °C to ensure formation of the perovskite. The region of interest focussed on small compositional variations around the $Ba_{0.8}Sr_{0.2}TiO_3$ target with Mn doping of up to 5 at%. The dielectric properties were tested under varying dc bias fields at three different frequencies (1, 10, 100 kHz) and tunabilities of 58.3 % and 57.3 % at 1 and 100 kHz, respectively, have been obtained between 0 and 45 kV mm^{-1} bias. Although the tunability has decreased by 7-8 % with respect to the undoped BST, one of the major advantages gained by Mn doping was to lower the dielectric loss and to allow stable dielectric performances at elevated frequencies. The material was also used in a co-planar waveguide phase shifter and was shown to operate at over 10 GHz with a low insertion loss of ~3.2 dB, a 12° phase shift was achieved with a small 10 V biasing voltage with excellent transmission characteristics.

Anions doping and multiple doping

So far, all approaches using HT-ePVD have focussed on cationic sites and their substitutions. Although most perovskites are oxygen perovskites, to the extent that the generic formula is often referred to as ABO_3, there are other elements in the periodic table which can go on the anionic site of the perovskite structure, such as fluorine, chlorine, bromine, iodine, sulphur and selenium. In fact, a favoured generic formula for perovskites is ABX_3.[29] Another possibility for anionic site is to mix or substitute the anions. Recently an organic-inorganic solar cell perovskite with a sulphur and iodine mixture has been reported.[87] A similar concept was used in 2013 when we have used the HT-ePVD approach to the synthesis and study of anion doping combined with A site substitutions in $Ba_xSr_{1-x}Ti_y(O,N)_{3-\delta}$ as tunable dielectrics. This was also extended into a study of substitutions on all sites with the investigation into the $(Ba_{0.8-x}Gd_xSr_{0.2})_{1+x}(Ti_{1-p}Zr_p)_{1-x}O_{3-z}N_z$.[82] In the case of the $Ba_xSr_{1-x}Ti_y(O,N)_{3-\delta}$, pure perovskite phases were obtained by in-situ crystallisation for a large range of compositions. Secondary phases are detected for compositions away from the tie-line with a tolerance factor in excess of 1.05. Significant improvements in the electrical characteristics of the materials were also obtained with an increase in dielectric constant when compared to the pure oxide perovskite and a tunability of 6.8 between 0 and 36 kV mm^{-1} at 1 kHz. Decreases in the dielectric losses were also seen under biases compared to the pure oxide perovskite with values of tan δ as low as 0.0032 at 36 kV mm^{-1} and 1 kHz. The ternary plot of dielectric constant shown in Figure 6 reveals a region where values between 900 and 1000 have been measured, this region corresponds to a higher concentration of barium than of strontium (similarly to what is obtain for the $Ba_xSr_{1-x}Ti_yO_{3-\delta}$ system) however it also corresponds to titanium concentrations slightly lower than the ideal 50 at% tie-line. This is the opposite to what is observed in the case of the $Ba_xSr_{1-x}Ti_yO_{3-\delta}$ system (see Figure 4). The difference has been observed repeatedly and it is not clear if the nitrogen is playing a direct role in this observation or if its influence is limited to the crystal growth, the oxynitride thin films were consistently found to have significant preferential orientation with a very strong (001) reflection. The levels of nitrogen measured by XPS in these samples is low, nonetheless the improvements in electrical performance are significant. Another aspect to notice is that the apparent hot spot of highest dielectric constant seem parallel to the Ti concentration for $Ba_xSr_{1-x}Ti_yO_{3-\delta}$ but deviates towards lower Ti levels in the $Ba_xSr_{1-x}Ti_y(O,N)_{3-\delta}$. Possible explanations involve oxygen vacancies, change in oxidation levels or site substitutions, further experiments would be required to further elucidate this. Finally the study of gadolinium and zirconium doping of the $Ba_xSr_{1-x}Ti_y(O,N)_{3-\delta}$ system involved multiple substitutions between Gd, Ba and Sr on the A-site, Zr and Ti on the B-site and nitrogen and oxygen on the anionic site. Using the in-situ direct crystallisation approach, the samples were deposited with a substrate temperature of 650 °C. A single perovskite phase was obtained for the compositional spread studied and although no improvements in dielectric constant, tunability and dielectric loss were observed, compared to the maxima found in the $Ba_xSr_{1-x}Ti_y(O,N)_{3-\delta}$, it was found that regions of low dielectric loss extended for a wider range of compositions.

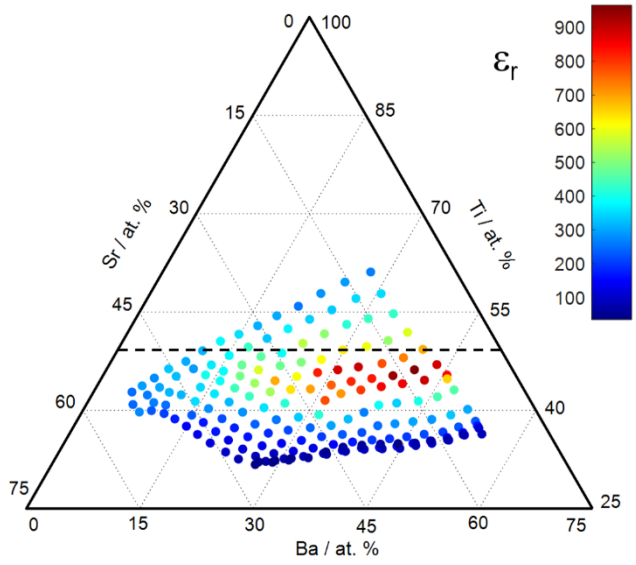

Figure 6: Dielectric constant at 1 kHz for the $Ba_xSr_{1-x}Ti_y(O,N)_{3-\delta}$ system, the dashed line represents the 50 at% Ti (results obtained as part of the work published by David *et al.*[82]).

Experimental Procedures for HT-ePVD studies

The syntheses took place a UHV system with a base pressure of $2x10^{-9}$ Torr by DCA Instruments. The elements (from 97% to 99.9% purity) were deposited from either Knudsen cells (25 cc or 40 cc) from DCA instruments or electron beam sources (40 cc) from Telemark, the gases were provided via a RF atom source from Oxford Applied Research with a 600 W RF power. The substrates used were either SSTOP (Si/SiO2/TiO2/Pt), AlOPt (sapphire/TiO2/Pt) or ITO electrochemical substrates.

All characterisations and screening were done, typically, as a 14x14 array of measurements, although arrays of 10x10, 12x12 and 8x8 have also been used.

Compositional characterisation was done using either an SEM equipped with an EDS system or Laser Ablation Inductively Coupled Plasma Mass Spectrometry (LA-ICPMS). X-ray diffraction was done using a Brucker Discovery D8 equipped with an Incoatec microsource Cu K_α and GADDS detector. XPS studies were done using a Spot XPS (ThermoFisher XR3 twin anode with Alpha 110 analyser and Advantage software). Electrical characterisations were done using an LCR meter (HP4284A), an Impedance Analyser (Solartron 1260A) and I-V source meters (Keithley) used in conjunction with a Signatone probestation. Electrochemical characterisation was carried out with samples specially deposited on 100 electrodes electrochemical arrays and tested using custom built cells, current followers and potentiostat.

Further information, specific to each system, about the experimental details can be found in the relevant published work. [4, 5, 77-82, 84, 85]

Conclusions

The use of High-Throughput evaporative Physical Vapour Deposition has been extensively used for the synthesis and study of perovskite thin films. The unique ability to control large compositional variations allows to gain an unrivalled insight into the material properties, by providing a large set of experimental points across the compositional space, compared to more classical approaches where only set of discreet compositions can be studied. The co-deposition, by condensation, of the constituent elements from vapour phases in vacuum, lead to a low energy route to phase formation which allow pure anion stoichiometric crystalline phases to be obtained at lower temperatures than in the case of more traditional approaches. The direct in-situ crystallisation route by deposition on substrates at elevated temperature is favoured but not always practical due to the low vapour pressures of some elements resulting in low residence times on the substrate. Our approach applied itself to substitution studies on both cationic sites as well as the anionic site and interpretation of the data obtained with respect to compositional space can also highlight unexpected sites substitutions. This approach is also unique in allowing to generate large datasets for many applications of interest, these relatively easily accessible experimental datapoints are essential in building databases for enabling the development of reliable algorithms to use with the developing field of machine learning. Finally, this approach has been extensively used for the synthesis and study of the perovskite class of materials, but it does not limit itself to these. Any crystal class, such as, for example, pyrochlores, spinels, garnets and delafossites, where systematic and gradual elemental substitutions are possible, presents an opportunity to deploy the HT-ePVD synthesis.

Conflicts of interest

There are no conflicts to declare.

Acknowledgements

The authors would like to acknowledge Dr Chris Vian for provision of support in informatics.

Notes and references

1. Mantle (geology), https://en.wikipedia.org/wiki/Mantle_(geology)).
2. A. Wagner, Everything you ever wanted to know about perovksite, Earth's most abundant type of mineral - that we almost never see, http://www.sciencemag.org/news/2017/11/everything-you-ever-wanted-know-about-perovskite-earth-s-most-abundant-type-mineral-we, 2019).
3. V. M. Goldschmidt, *Naturwissenschaften*, 1926, **14**, 477-485.
4. B. E. Hayden and F. K. Rogers, *Journal of Electroanalytical Chemistry*, 2018, **819**, 275-282.
5. K. Bradley, K. Giagloglou, B. E. Hayden, H. Jungius and C. Vian, *Chemical Science*, 2019, DOI: 10.1039/C9SC00412B.
6. N. Rashid, A. A. Samat, A. A. Jais, M. R. Somalu, A. Muchtar, N. A. Baharuddin and W. Isahak, *Ceramics International*, 2019, **45**, 6605-6615.
7. S. P. Jiang, *International Journal of Hydrogen Energy*, 2019, **44**, 7448-7493.
8. J. Hwang, R. R. Rao, L. Giordano, Y. Katayama, Y. Yu and Y. Shao-Horn, *Science*, 2017, **358**, 751-756.
9. Z. Li, M. Yang, J.-S. Park, S.-H. Wei, J. J. Berry and K. Zhu, *Chemistry of Materials*, 2016, **28**, 284-292.
10. J. Lei, F. Gao, H. X. Wang, J. Li, J. X. Jiang, X. Wu, R. R. Gao, Z. Yang and S. Z. Liu, *Solar Energy Materials and Solar Cells*, 2018, **187**, 1-8.
11. P. F. Luo, S. W. Zhou, W. Xia, J. G. Cheng, C. X. Xu and Y. W. Lu, *Advanced Materials Interfaces*, 2017, **4**.
12. V. Zardetto, B. L. Williams, A. Perrotta, F. Di Giacomo, M. A. Verheijen, R. Andriessen, W. M. M. Kessels and M. Creatore, *Sustainable Energy & Fuels*, 2017, **1**, 30-55.
13. A. Ioakeimidis, C. Christodoulou, M. Lux-Steiner and K. Fostiropoulos, *Journal of Solid State Chemistry*, 2016, **244**, 20-24.
14. D. Szczesniak, A. Z. Kaczmarek, R. Szczesniak, S. V. Turchuk, H. Zhao and E. A. Drzazga, *Modern Physics Letters B*, 2018, **32**.
15. A. Aqeel, N. Akhtar, A. O. Polyakov, P. Rudolf and T. T. M. Palstra, *Apl Materials*, 2018, **6**.
16. Y. Tojo, T. Shibuya, T. Nakamura, K. Shoji, H. Fujioka, M. Matoba, S. Yasui, M. Itoh, S. Iimura, H. Hiramatsu, H. Hosono, S. Hirai, W. Mao, S. Kitao, M. Seto and Y. Kamihara, *Journal of Physics-Condensed Matter*, 2019, **31**.
17. X. Ma, A. Firdous, L. Zhang, S. J. Wu, J. X. Zhang, L. J. Liu, Y. Wang, J. L. Geng, J. L. Sun, G. B. Li, F. H. Liao and J. H. Lin, *Chemistryselect*, 2019, **4**, 3135-3139.
18. A. H. Khan, S. Atiq, A. Mahmood, S. M. Ramay, S. K. Abbas and S. Naseem, *Ceramics International*, 2018, **44**, 14677-14685.
19. I. R. Reddy, P. M. Oppeneer and K. Tarafder, *Physical Review B*, 2018, **98**.
20. N. D. Sharma, A. Mahajan, M. K. Verma, N. Choudhary, S. Sharma and D. Singh, *Ionics*, 2019, **25**, 1271-1279.
21. J. Xing, Y. B. Zhao, M. Askerka, L. N. Quan, X. W. Gong, W. J. Zhao, J. X. Zhao, H. R. Tan, G. K. Long, L. Gao, Z. Y. Yang, O. Voznyy, J. Tang, Z. H. Lu, Q. H. Xiong and E. H. Sargent, *Nature Communications*, 2018, **9**.
22. Z. H. Wei and J. Xing, *Journal of Physical Chemistry Letters*, 2019, **10**, 3035-3042.
23. G. C. Xie, C. B. Jiang, J. H. Wang, C. H. Mai, G. H. Huang, Y. W. Ma, J. Wang, J. B. Peng and Y. Cao, *Organic Electronics*, 2019, **71**, 58-64.
24. Q. Zhang, Y. Lu, Z. W. Liu, H. T. Yu, Y. Duan, L. H. Liu, S. F. Chen and W. Huang, *Organic Electronics*, 2019, **72**, 30-38.
25. S. Q. Luo, J. F. Wang, B. Yang and Y. B. Yuan, *Frontiers of Physics*, 2019, **14**.
26. H. Zhu, Y. Fu, F. Meng, X. Wu, Z. Gong, Q. Ding, M. V. Gustafsson, M. T. Trinh, S. Jin and X. Y. Zhu, *Nature Materials*, 2015, **14**, 636.
27. K. Wang, S. Wang, S. Xiao and Q. Song, *Advanced Optical Materials*, 2018, **6**, 1800278.

28. J. Rodel, W. Jo, K. T. P. Seifert, E. M. Anton, T. Granzow and D. Damjanovic, *Journal of the American Ceramic Society*, 2009, **92**, 1153-1177.
29. D. G. Schlom, L. Q. Chen, X. Q. Pan, A. Schmehl and M. A. Zurbuchen, *Journal of the American Ceramic Society*, 2008, **91**, 2429-2454.
30. K. J. Stanly, I. P. Selvam and V. Kumar, *Materials Letters*, 1999, **40**, 118-123.
31. H. L. Chen, J. Wang, X. Q. Yin, C. Xing, J. Z. Li, H. Y. Qiao and F. Shi, *Materials Research Express*, 2019, **6**.
32. M. Y. Yeh, J. H. Li, S. H. Chang, S. Y. Lee and H. C. Huang, *Modern Physics Letters B*, 2019, **33**.
33. I. C. Kaya, V. Kalem and H. Akyildiz, *International Journal of Applied Ceramic Technology*, 2019, **16**, 1557-1569.
34. M. Ranjbar, M. E. Ghazi and M. Izadifard, *Journal of Materials Science-Materials in Electronics*, 2019, **30**, 10619-10629.
35. T. K. Dhiman and S. Singh, *Physica Status Solidi a-Applications and Materials Science*, 2019, **216**.
36. C. L. Diao, H. Li, Y. Yang, H. Hao, Z. H. Yao and H. X. Liu, *Ceramics International*, 2019, **45**, 11784-11791.
37. H. Gao, X. Meng, Y. L. Du and X. Y. Gao, *Thin Solid Films*, 2019, **682**, 37-43.
38. P. Pal, S. Saha, A. Banik, A. Sarkar and K. Biswas, *Chemistry-a European Journal*, 2018, **24**, 1811-1815.
39. A. R. Vazquez-Olmos, M. E. Sanchez-Vergara, A. L. Fernandez-Osorio, A. Hernandez-Garcia, R. Y. Sato-Berru and J. R. Alvarez-Bada, *Journal of Cluster Science*, 2018, **29**, 225-233.
40. B. A. Rosales, L. Wei and J. Vela, *Journal of Solid State Chemistry*, 2019, **271**, 206-215.
41. M. Dragomir, M. Otonicar, M. Vrabelj, L. Fulanovic, S. Drnovsek, T. Rojac and B. Malic, *Journal of the European Ceramic Society*, 2019, **39**, 1837-1845.
42. G. Demazeau, *Phase Transitions*, 1996, **58**, 43-56.
43. K. H. Dahmen and M. W. Carris, *Chemical Vapor Deposition*, 1997, **3**, 27-+.
44. M. Reinke, Y. Kuzminykh, F. Eltes, S. Abel, T. LaGrange, A. Neels, J. Fompeyrine and P. Hoffmann, *Advanced Materials Interfaces*, 2017, **4**.
45. E. Ahvenniemi, M. Matvejeff and M. Karppinen, *Dalton Transactions*, 2015, **44**, 8001-8006.
46. C. K. Cheng, L. B. Young, K. Y. Lin, Y. H. Lin, H. W. Wan, G. J. Lu, M. T. Chang, R. F. Cai, S. C. Lo, M. Y. Li, C. H. Hsu, J. Kwo and M. Hong, *Microelectronic Engineering*, 2017, **178**, 125-127.
47. M. D. McDaniel, T. Q. Ngo, S. Hu, A. Posadas, A. A. Demkov and J. G. Ekerdt, *Applied Physics Reviews*, 2015, **2**.
48. J. H. Shim, H. J. Choi, Y. Kim, J. Torgersen, J. An, M. H. Lee and F. B. Prinz, *Journal of Materials Chemistry C*, 2017, **5**, 8000-8013.
49. A. Cyza, L. Cieniek and A. Kopia, *Archives of Metallurgy and Materials*, 2016, **61**, 1063-1067.
50. M. J. Han, Y. J. Wan, D. S. Ma, Y. L. Zhu, Y. L. Tang, Y. Liu, N. B. Zhang, J. Y. Ma and X. L. Ma, *Acta Materialia*, 2018, **145**, 220-226.
51. K. K. James, B. Satish and M. K. Jayaraj, in *Optoelectronic Materials and Thin Films*, ed. M. K. Jayaraj, 2014, vol. 1576, pp. 212-214.
52. M. Jelinek, P. Vanek, Z. Tolde, E. Buixaderas, T. Kocourek, V. Studnicka, J. Drahokoupil, J. Petzelt, J. Remsa and M. Tyunina, *Materials Science & Engineering C-Materials for Biological Applications*, 2017, **70**, 334-339.
53. S. Jun, C. Yang and J. Lee, *Science of Advanced Materials*, 2015, **7**, 102-106.
54. D. H. Kim, L. Bi, N. M. Aimon, P. Jiang, G. F. Dionne and C. A. Ross, *Acs Combinatorial Science*, 2012, **14**, 179-190.
55. A. Singh, Z. R. Khan, P. M. Vilarinho, V. Gupta and R. S. Katiyar, *Materials Research Bulletin*, 2014, **49**, 531-536.
56. X. Y. Sun, C. Zhang, N. M. Aimon, T. Goto, M. Onbasli, D. H. Kim, H. K. Choi and C. A. Ross, *Acs Combinatorial Science*, 2014, **16**, 640-646.
57. K. R. Talley, S. C. Barron, N. Nguyen, W. Wong-Ng, J. Martin, Y. L. Zhang and X. Song, *Solid State Sciences*, 2017, **64**, 7-12.
58. M. Biswas and P. C. Su, *Chemical Solution Deposition Technique of Thin-Film Ceramic Electrolytes for Solid Oxide Fuel Cells*, 2017.
59. G. He, C. Peng, M. Z. He, J. H. Hong, H. F. Li and Y. S. Gong, *Functional Materials Letters*, 2013, **6**.
60. H. B. Cheng, H. Hida, J. Ouyang and I. Kanno, *Ceramics International*, 2017, **43**, 1597-1601.
61. P. Ratanapreechachai, I. Kanno, M. Sato and Ieee, in *Proceedings of the 2012 Fifth International Conference on Emerging Trends in Engineering and Technology*, 2012, DOI: 10.1109/icetet.2012.15, pp. 44-47.
62. K. Alberi, M. B. Nardelli, A. Zakutayev, L. Mitas, S. Curtarolo, A. Jain, M. Fornari, N. Marzari, I. Takeuchi, M. L. Green, M. Kanatzidis, M. F. Toney, S. Butenko, B. Meredig, S. Lany, U. Kattner, A. Davydov, E. S. Toberer, V. Stevanovic, A. Walsh, N. G. Park, A. Aspuru-Guzik, D. P. Tabor, J. Nelson, J. Murphy, A. Setlur, J. Gregoire, H. Li, R. J. Xiao, A. Ludwig, L. W. Martin, A. M. Rappe, S. H. Wei and J. Perkins, *Journal of Physics D-Applied Physics*, 2019, **52**.
63. R. Armiento, B. Kozinsky, G. Hautier, M. Fornari and G. Ceder, *Physical Review B*, 2014, **89**.
64. A. Jain, O. Voznyy and E. H. Sargent, *Journal of Physical Chemistry C*, 2017, **121**, 7183-7187.
65. T. Nakajima and K. Sawada, *Journal of Physical Chemistry Letters*, 2017, **8**, 4826-4831.
66. R. Sarmiento-Perez, T. F. T. Cerqueira, S. Korbel, S. Botti and M. A. L. Marques, *Chemistry of Materials*, 2015, **27**, 5957-5963.
67. K. Sawada and T. Nakajima, *Apl Materials*, 2018, **6**.
68. Q. D. Sun and W. J. Yin, *Journal of the American Chemical Society*, 2017, **139**, 14905-14908.
69. K. S. Yang, *Chinese Physics B*, 2018, **27**.
70. Z. Y. Zhang, R. W. Zhang, X. R. Li, K. Koepernik, Y. G. Yao and H. B. Zhang, *Journal of Physical Chemistry Letters*, 2018, **9**, 6224-6231.
71. I. M. Abdel-Motaleb, P. Navuduri, Y. Z. Yoo, O. Chmaissem and J. H. Song, *International Journal of Applied Ceramic Technology*, 2013, **10**, E159-E166.
72. S. Fujino, M. Murakami, V. Anbusathaiah, S. H. Lim, V. Nagarajan, C. J. Fennie, M. Wuttig, L. Salamanca-Riba and I. Takeuchi, *Applied Physics Letters*, 2008, **92**.
73. L. Luo, Z. H. Xiong, N. G. Zhou and H. P. Zhang, in *Advanced Materials and Processes Ii, Pts 1-3*, eds. H. B. Ji, Y. Chen and S. Z. Chen, 2012, vol. 557-559, pp. 674-+.
74. C. Peng, D. S. Zhao, G. He, M. Z. He, J. H. Hong, H. F. Li and Y. S. Gong, *Functional Materials Letters*, 2011, **4**, 231-235.

75. R. Pullar, Y. Zhang, L. F. Chen, S. F. Yang, J. Evans, A. Salak, D. Kiselev, A. Kholkin, V. Ferreira and N. M. Alford, *Journal of Electroceramics*, 2009, **22**, 245-251.
76. J. C. H. Rossiny, J. Julis, S. Fearn, J. A. Kilner, Y. Zhang, L. F. Chen, S. F. Yang and J. R. G. Evans, *Solid State Ionics*, 2008, **179**, 1085-1089.
77. P. S. Anderson, S. Guerin, B. E. Hayden, Y. Han, M. Pasha, K. R. Whittle and I. M. Reaney, *Journal of Materials Research*, 2009, **24**, 164-172.
78. P. S. Anderson, S. Guerin, B. E. Hayden, M. A. Khan, A. J. Bell, Y. Han, M. Pasha, K. R. Whittle and I. M. Reaney, *Applied Physics Letters*, 2007, **90**.
79. M. S. B. Darby, D. V. Karpinsky, J. Pokorny, S. Guerin, A. L. Kholkin, S. Miao, B. E. Hayden and I. M. Reaney, *Thin Solid Films*, 2013, **531**, 56-60.
80. M. S. B. Darby, S. Guerin, B. E. Hayden, H. J. Schreiner and S. Yakovlev, *Journal of Applied Physics*, 2013, **113**.
81. B. E. Hayden and S. Yakovlev, *Thin Solid Films*, 2016, **603**, 108-114.
82. A. David, S. Guerin, B. E. Hayden, R. Noble, J. P. Soulie, C. Vian, I. P. Koutsaroff, S. Higai, N. Tanaka, T. Konoike, A. Ando, H. Takagi, T. Yamamoto, T. Fukura and H. Ieki, *Crystal Growth & Design*, 2014, **14**, 523-532.
83. I. Bakaimi, X. L. He, S. Guerin, N. Z. I. Hashim, Q. Luo, I. M. Reaney, S. Gao, B. E. Hayden and C. H. K. de Groot, *Journal of Materials Chemistry C*, 2018, **6**, 6222-6228.
84. M. S. Beal, B. E. Hayden, T. Le Gall, C. E. Lee, X. J. Lu, M. Mirsaneh, C. Mormiche, D. Pasero, D. C. A. Smith, A. Weld, C. Yada and S. Yokoishi, *Acs Combinatorial Science*, 2011, **13**, 375-381.
85. S. Guerin and B. E. Hayden, *Journal of Combinatorial Chemistry*, 2006, **8**, 66-73.
86. S. Stramare, V. Thangadurai and W. Weppner, *Chemistry of Materials*, 2003, **15**, 3974-3990.
87. R. Nie, A. Mehta, B.-w. Park, H.-W. Kwon, J. Im and S. I. Seok, *Journal of the American Chemical Society*, 2018, **140**, 872-875.